materials

MDPI

Article

Synthesis of Tungsten-Doped Vanadium Dioxide Using a Modified Polyol Method Involving 1-Dodecanol

Yonghyun Lee [1], Sang Won Jung [1], Sang Hwi Park [2], Jung Whan Yoo [2] and Juhyun Park [1,*]

[1] Department of Intelligent Energy and Industry, School of Chemical Engineering and Materials Science, Chung-Ang University, Seoul 06974, Korea; lovembnb@cau.ac.kr (Y.L.); jung11361@naver.com (S.W.J.)
[2] KNW R&D Center, Gyeonggi-do 10832, Korea; kunchs@knwkorea.com (S.H.P.); jwyoo@knwkorea.com (J.W.Y.)
* Correspondence: jpark@cau.ac.kr; Tel.: +82-2-820-5735

Received: 20 October 2020; Accepted: 25 November 2020; Published: 27 November 2020

Abstract: The doping of tungsten into VO_2 (M) via a polyol process that is based on oligomerization of ammonium metavanadate and ethylene glycol (EG) to synthesize a vanadyl ethylene glycolate (VEG) followed by postcalcination was carried out by simply adding 1-dodecanol and the tungsten source tungstenoxytetrachloride ($WOCl_4$). Tungsten-doped VEGs (W-VEGs) and their calcinated compounds (W_xVO_2) were prepared with varying mixing ratios of EG to 1-dodecanol and $WOCl_4$ concentrations. Characterizations of W-VEGs by powder X-ray diffraction, differential scanning calorimetry, scanning electron microscopy, and infrared and transmittance spectroscopy showed that tungsten elements were successfully doped into W_xVO_2, thereby decreasing the metal-insulator transition temperature from 68 down to 51 °C. Our results suggested that $WOCl_4$ variously combined with 1-dodecanol might interrupt the linear growth of W-VEGs, but that such an interruption might be alleviated at the optimal 1:1 mixing ratio of EG to 1-dodecanol, resulting in the successful W doping. The difference in the solar modulations of a $W_{0.0207}VO_2$ dispersion measured at 20 and 70 °C was increased to 21.8% while that of a pure VO_2 dispersion was 2.5%. It was suggested that $WOCl_4$ coupled with both EG and 1-dodecanol at an optimal mixing ratio could improve the formation of W-VEG and W_xVO_2 and that the bulky dodecyl chains might act as defects to decrease crystallinity.

Keywords: vanadium oxide; thermochromic; nanoparticles; tungsten doping; smart windows

1. Introduction

Smart windows that use the thermochromic property of vanadium dioxide (VO_2) have been highlighted as a promising energy saving technology due to their selective control over the transmission of heat rays that enhances energy saving efficiency [1]. At 68 °C or below, VO_2 has a monoclinic structure (M) with a semiconducting property, and at temperatures above 68 °C, its crystal structure is transformed to a tetragonal rutile structure, accompanying a change in its electrical property from semiconducting to metallic [2]. This metal-insulator transition (MIT) enables VO_2 to selectively reflect near-infrared light (NIR) due to its metallic property above its MIT temperature while transmitting visible light [3]. To practically apply the thermochromic property of VO_2 to smart windows that can control sunlight transmission at room temperature, decreasing the MIT temperature of VO_2 down to around room temperature is very much required. The doping of VO_2 (M) with tungsten (W) atoms has been a promising route for reducing the MIT temperature of VO_2 (M) [4–7]. When tungsten atoms are doped to the VO_2, it is expected that the original V^{4+}-V^{4+} pairs in VO_2 (M) are converted to V^{3+}-V^{4+} and V^{3+}-W^{6+} pairs by electron donation from W to the neighboring V ions. As a result,

the concentration of free electrons is increased via electron donation, and the monoclinic structure is distorted due to the insertion of larger doped W^{6+} ions with an ionic radius of 64 pm than V^{4+} ions with an ionic radius of 49.5 pm. Thus, the MIT temperature of pristine VO_2 is decreased, making W_xVO_2 (M) an ideal candidate for thermochromic window materials as it can reflect NIR at room temperature while transmitting visible light [8,9].

A variety of methods, including hydrothermal synthesis with an autoclave at a high pressure [10], chemical vapor deposition (CVD) [11], sputtering [12,13], and ion implantation [14], have been utilized to synthesize W_xVO_2 (M). However, these methods require complicated experimental parameter controls or special devices, thereby restricting the extension of these methods to large-scale production at a low cost. Thus, it is highly necessary to develop a convenient process that utilizes atmospheric pressure in air at a low processing temperature. A candidate method for resolving these issues is the thermolysis of vanadyl glycolate to synthesize VO_2 (M) [15,16]. In this method, an alcohol with two or more hydroxyl groups and high boiling points, such as ethylene glycol (EG) with a boiling point of 197 °C, is mixed with a cheap vanadium precursor, such as ammonium metavanadate (NH_4VO_3), and the resulting solution mixture is heated over 160 °C in atmospheric air followed by thermolysis of precipitates at a low pyrolytic temperature of 200 °C to produce VO_2 (M) (Scheme 1). In this polyol method, EG works as a stabilizer that limits particle growth and prevents aggregation [17], as a coupling agent that can further lead vanadyl ethyleneglycol glycolate (VEG) to oligomer with a repeat unit of $VO(OCH_2CH_2O)$ [18], and as a reducing agent when the VEG is calcinated [19]. The crystal structure of VEG can also be depicted by the one-dimensional chain of the VO_5 square pyramids in the $VO(OCH_2CH_2O)$ structure by edge sharing (Scheme 1) [19]. When using this method to make VEG, special devices are not required, and subsequent calcination can be carried out via a conventional sintering process, thereby suggesting its possibility for mass production at a low cost. Although the polyol method shows great potential for the facile synthesis of W_xVO_2, it is difficult to find reports about the polyol method being applied to synthesize W_xVO_2 nanoparticles. This lack of research seems to be because a special synthesis for tungsten precursors that can be coupled within VEG is necessary or because the insertion of the large W^{6+} ions into the monoclinic VO_2 (M) at an atmospheric pressure is difficult. Thus, the synthesis of W_xVO_2 using the polyol method via thermolysis in atmospheric air remains challenging.

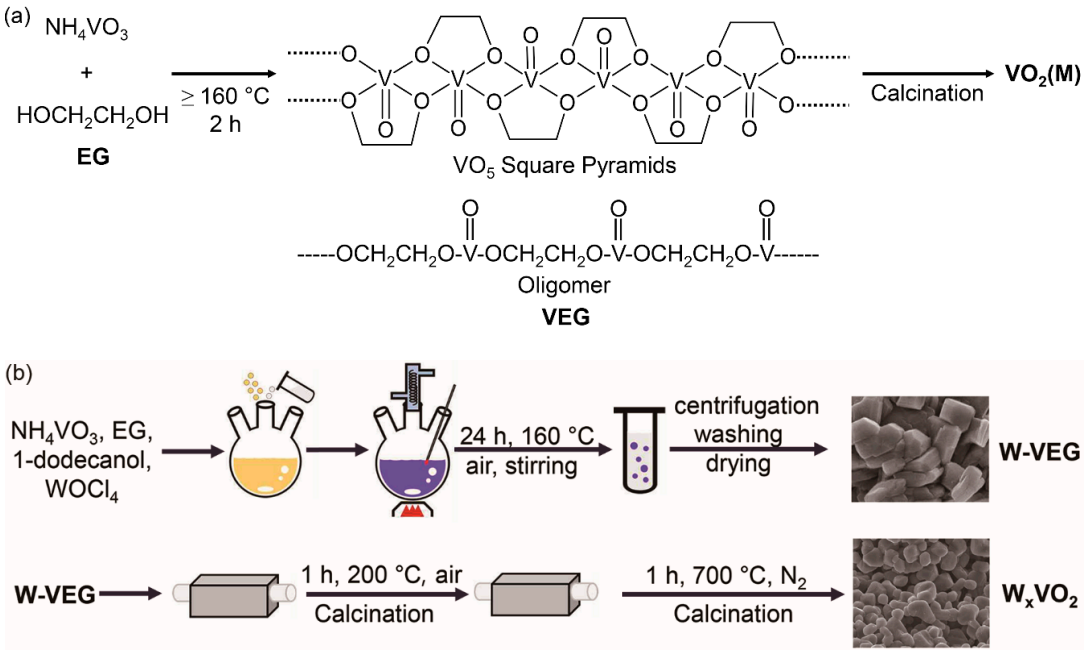

Scheme 1. (**a**) Reaction for the preparation of VO_2 (M) via a polyol method and (**b**) a schematic illustration of the W-VEG synthesis and calcination.

In this study, we present a modified polyol method using 1-dodecanol as an additive to synthesize W_xVO_2 (M). 1-Dodecanol has a boiling point of 259 °C, which is high enough for the polyol method, and can act as both the solvent and capping agent, as shown in inorganic nanoparticle synthesis [20]. Unlike the original polyol method, we found that tungsten could be doped into VO_2 (M) with the addition of 1-dodecanol, thereby reducing the MIT temperature of the resulting W_xVO_2 (M). We investigated the influence of the mixing ratios of EG and 1-dodecanol and the amounts of tungsten precursor on the synthesis of W_xVO_2. Our results suggest a procedure to dope tungsten into VO_2 (M) via the polyol method.

2. Materials and Methods

2.1. Materials

NH_4VO_3 and tungsten(VI) oxytetrachloride ($WOCl_4$) were purchased from Sigma-Aldrich Co. (St. Louis, MO, USA). EG and 1-dodecanol were purchased from Alfa Aesar (Lancashire, United Kingdom). Ethanol was obtained from SamChun Pure Chemicals Co. (Seoul, South Korea). All the reagents used in this study were used as received.

2.2. Synthesis

To first synthesize tungsten-doped VEG (W-VEG), NH_4VO_3 (1.17 g, 10 mmol), 1-dodecanol (33.17 g, 17.8 mmol), and EG (11.05 g, 17.8 mmol) were added to a three-necked round-bottom flask and mixed with stirring. To this mixture solution, a pre-determined amount of $WOCl_4$ (0.094 g [0.277 mmol, 2.77 mol% to NH_4VO_3], 0.188 g [0.553 mmol, 5.53 mol%), and 0.377 g [1.109 mmol, 11.08 mol%]) was added, and the resulting reaction mixture was heated to 160 °C at a ramping rate of 5 °C/min and stirred for 2 h. Then, the mixture with a purple color was naturally cooled down to room temperature. The precipitate was collected by centrifuging the solution at 8000 rpm for 15 min to remove the excess 1-dodecanol and EG. The collected purple powder was washed with ethanol, filtered to obtain W-VEG powder, and dried in a vacuum for 24 h at room temperature.

The W-VEG powder was calcinated at 200 °C for 1 h in a box furnace in atmospheric air to become W_xVO_y (M). After cooling to room temperature, W_xVO_y (M) was calcinated again at 700 °C (10 °C/min) for 1 h in a tube furnace in a vacuum to obtain W_xVO_y (M).

2.3. Characterization

The crystal structures of the W_xVO_y (M) were verified by an X-ray diffractometer (XRD, Bruker-AXS NEW D8 Advance, Billerica, MA, USA). The MIT behaviors of the W_xVO_y (M) were investigated using a differential scanning calorimeter (DSC Q-600; TA Instruments, New Castle, DE, USA) for analysis in the range −20–130 °C at a heating rate of 10 °C/min. Morphological observations of the nanostructures were conducted on a field-emission scanning electron microscope (FE-SEM; SIGMA, Carl Zeiss, Germany). The thermochromic properties of W_xVO_y (M) were measured using UV-Vis-NIR spectroscopy (V-770, JASCO, Tokyo, Japan) in the range of 300–2500 nm. Before measuring the UV-Vis-NIR spectra, the W_xVO_y (M) powder (0.02 g) was added in 5 mL of ethanol, and the solution was dispersed for 1 h under ultrasonication to make the suspension and placed in a quartz cell with 1 mm light path. The FT-IR spectra were recorded using a high-vacuum FT-IR spectrometer system in a spectral range of 4000 to 400 cm^{-1} (Vertex 80V, operated by the Korea Basic Science Institute at Busan, Bruker Co., Billerica, MA, USA). KBr pellets that were prepared with 1 mg of samples and 15 mg of KBr were used for measurements in a vacuum. The compositions of W_xVO_y were determined by using an Inductively Coupled Plasma Atomic Emission Spectrometer (ICP-AES; Jobin Yvon Ultima2, operated by the Korea Basic Science Institute at Seoul; HORIBA, Edison, NJ, USA).

3. Results and Discussion

We used $WOCl_4$ as a tungsten precursor to synthesize W_xVO_2 (M) via the polyol method based on ammonium metavanadate and EG because $WOCl_4$ could be readily combined with EG via an exothermic reaction between $WOCl_4$ and hydroxyl groups that make byproducts of HCl. Thus, one might expect that $WOCl_4$ combined with EG participates in the formation of VEG, thereby resulting in the insertion of tungsten atoms into VO_2 (M) during calcination. However, when 2.77 mol% of $WOCl_4$ to NH_4VO_3 was added into the reaction mixture of ammonium metavanadate and EG at the 1:0 mixing ratio of EG to 1-dodecanol, the final product gained after calcination did not show a highly crystalline structure in its XRD pattern, as shown in Figure 1a. Additionally, the XRD pattern was not matched with that of VO_2 (M). This result can be ascribed to the incomplete synthesis of linear VEG via a condensation reaction between NH_4VO_3 and EG because $WOCl_4$ with four reactive W-Cl functionalities to EGs can interrupt the formation of the linear VEG.

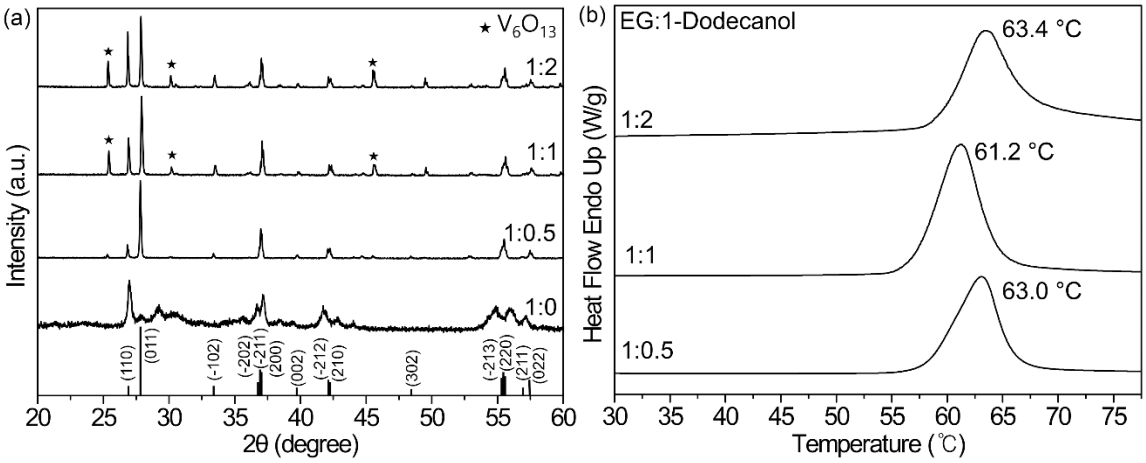

Figure 1. (**a**) XRD patterns and (**b**) DSC thermograms of tungsten-doped vanadium oxides obtained with varying molar mixing ratios of EG to 1-dodecanol at 1:0, 1:0.5, 1:1 and 1:2.

We presumed that the simple addition of 1-dodecanol as a co-solvent could resolve this issue because 1-dodecanol might act as a partial capping agent for the highly reactive W-Cl functionality in $WOCl_4$. To investigate the capping effect of 1-dodecanol on $WOCl_4$, we carried out the synthesis of W_xVO_2 by varying the molar mixing ratio of EG to 1-dodecanol at 1:0.5, 1:1, and 1:2 at fixed amounts of NH_4VO_3 to $WOCl_4$ at 10 and 0.277 mmol, respectively. Figure 1a shows the XRD patterns of the tungsten-doped vanadium oxides produced by controlling the molar ratio of EG:1-dodecanol. The observed diffraction peaks at all three ratios of 1:0.5, 1:1 and 1:2 indicate the monoclinic vanadium dioxide VO_2 (M) crystal structure reported in JCPDS No. 43-1051 [21]. Particularly, well-developed crystallinity was seen in the main VO_2(M) peaks at 2θ angles of 26.8°, 27.8° 33.4°, 37.0°, 39.8°, 42.1°, 42.2°, 55.5°, and 57.4° for (110), (011), (−102), (−202; −211; 200), (002), (−212; 210), (−213; 220; 211), and (022) planes, respectively. However, diffraction peaks of V_6O_{13} at 2θ = 25.3°, 30.1°, and 45.6° for (101), (400), and (005), respectively, were also clearly observed in the XRD patterns of the compounds synthesized at ratios of 1:1 and 1:2, and were in agreement with the reference data (JCPDS No. 25-1251) [22]. The appearance of the oxidized V_6O_{13} peaks originates from the increase in oxygen contents in W-VEG as the molar ratio of 1-dodecanol increases. It appears that excess oxygen atoms incorporated into the VO_2 structure chemically interact with vanadium atoms to form a new oxidation state of V_6O_{13}, as stated in literature [23].

The decrease in MIT temperatures with the addition of tungsten precursors in varying molar ratios of EG to 1-dodecanol at the fixed amount of $WOCl_4$ to NH_4VO_3 was confirmed by measuring the DSC thermogram. In Figure 1b, the DSC curves show that the MIT temperatures were 63.03, 61.23, and 63.44 °C at mixing ratios of 1:0.5, 1:1, and 1:2 for EG to 1-dodecanol. These results show an obvious

drop from 68 °C, the original MIT temperature of VO_2 (M), and indicate successful tungsten doping via the polyol method. Furthermore, it should be noted that W_xVO_2 prepared from the 1:1 mixture of EG to 1-dodecanol has the lowest MIT temperature, although the fixed amount of $WOCl_4$ was used for all calcinated samples.

To investigate the origination of these variations in the MIT temperatures, we measured SEM images of VEG synthesized without using 1-dodecanol and $WOCl_4$ as a reference and W-VEGs prepared with varying mixing ratios of EG to 1-dodecanol at the fixed $WOCl_4$ concentration of 2.77 mol% relative to NH_4VO_3 (Figure 2). The SEM images of VEG in Figure 2a looks like a mixture of square rods at the nano- and micrometer scales, which is similar to nanorods found in the literature [24]. This morphology reflects VEG crystals based on one dimensional chain of square pyramids sharing edges with the formula $VO(OCH_2CH_2O)$ [19], as shown in Scheme 1. When 1-dodecanol was not used, the SEM image of W-VEG, as can be seen in Figure 2b, showed microcrystals with rod-like morphologies and a square cross section. The side length of the square cross section was around 1 μm. This morphology did not significantly deviate from that of VEG without using the tungsten precursor, as can be seen in Figure 2a. With the addition of 1-dodecanol at 1:0.5 and 1:2, as shown in Figure 2c,e, the edges of the crystals were smeared, and the resulting morphology was a mixture of rods and smeared aggregates. The SEM image at 1:1 shown in Figure 2d shows morphologies with sharp edges, but the sizes and lengths of the microcrystals were significantly decreased in comparison to those at a 1:0 ratio of 1-dodecanol.

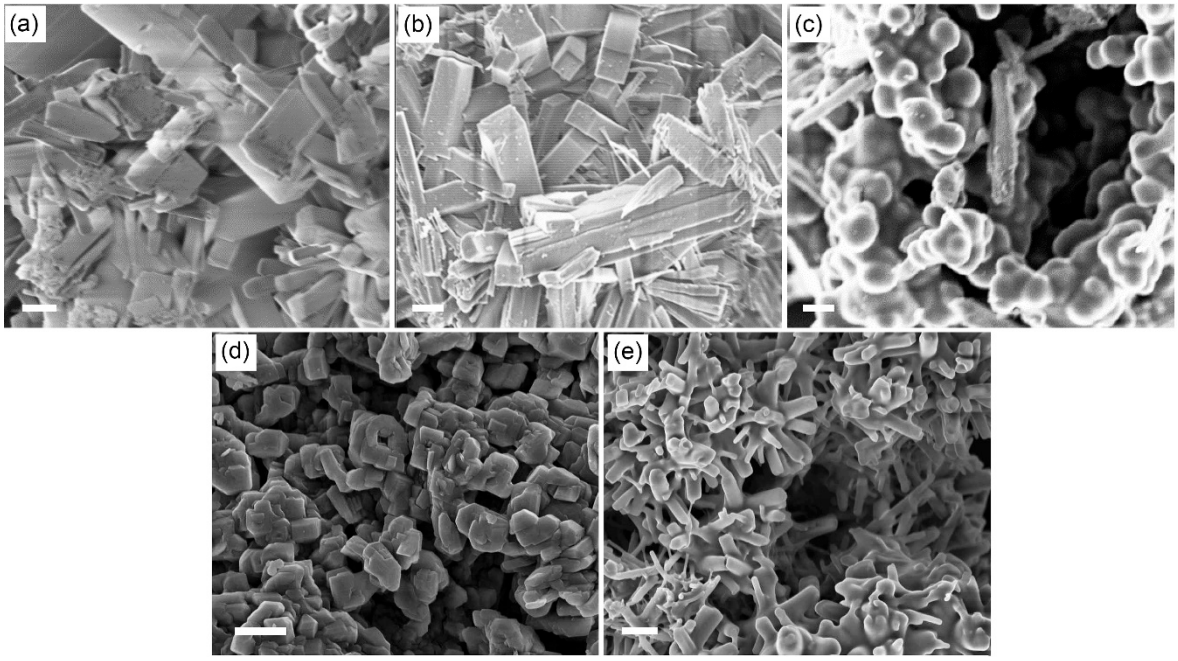

Figure 2. FE-SEM images of VEG (**a**) and W-VEGs (**b**–**e**) obtained with different mixing ratios of EG to 1-dodecanol at (**a**) 1:0 without using $WOCl_4$, (**b**) 1:0, (**c**) 1:0.5, (**d**) 1:1, and (**e**) 1:2 at a fixed $WOCl_4$ concentration of 2.77 mol% relative to NH_4VO_3, respectively. (scale bar = 1 μm).

One hypothesis to explain the variation in the morphologies of W-VEG microcrystals is that $WOCl_4$ reacted with 1-dodecanol, which significantly influenced the crystal morphologies. The reaction between NH_4VO_3 and EG is like the oligomerization of two monomers, resulting in VEG with a one-dimensional chain of VO_5 square pyramids, as shown in Scheme 1 and the literature [18]. Our results suggest that the $WOCl_4$ combined with 1-dodecanol might interrupt the growth of VEG in one dimension, resulting in the decrease in tungsten doping after calcination of the W-VEG, and when at the 1:1 molar mixing ratio, such an interruption might be alleviated. In the mixture of EG and 1-dodecanol, $WOCl_4$ can form many different chemical structures shown in Scheme 2. Without using 1-dodecanol, species I, II, and III are primarily formed, and species I might hinder the formation of the

one-dimensional chain of the VO_5 square pyramids due to its multiple functionalities. Species IV, V, VI, and VII, which can be produced by the reaction of $WOCl_4$ with both of EG and 1-dodecanol, should also significantly influence the final morphologies of W-VEGs. In particular, species V might be the main product of the reaction between $WOCl_4$ and the mixture of EG and 1-dodecanol at a 1:1 ratio due to the statistically equal opportunity for the reaction, which occurs only if the reactivities of $WOCl_4$ to EG and 1-dodecanol are identical; this in turn can be responsible for the improved tungsten doping.

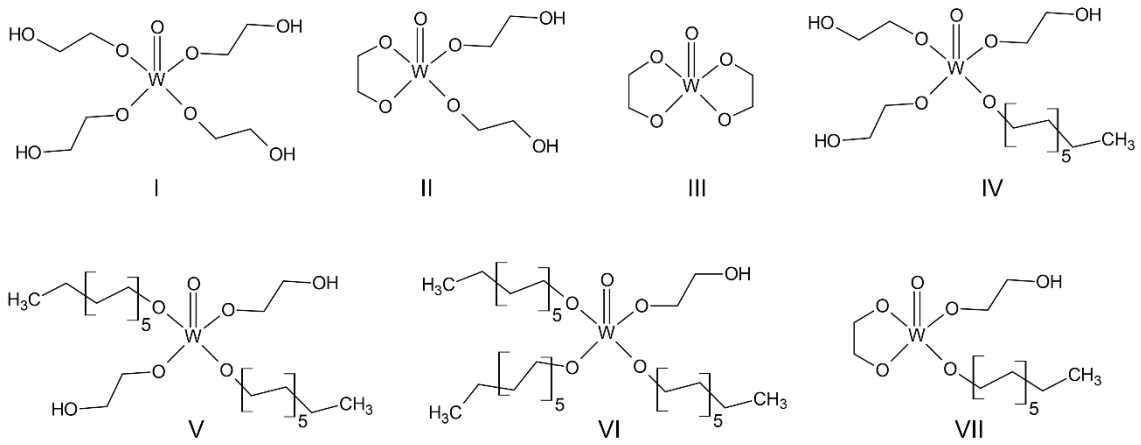

Scheme 2. Chemical structures of species that can be formed via reactions of $WOCl_4$ with a mixture of EG and 1-dodecanol at different mixing ratios.

To further investigate the credibility of our hypothesis and speculations and the effects of the addition of 1-dodecanol, we examined the FT-IR spectra of W-VEGs prepared at different mixing ratios of EG to 1-dodecanol. The FT-IR spectra of W-VEGs shown in Figure 3a in a range of 4000 to 400 cm^{-1} clearly present IR bands of O-H stretching (~ 3450 cm^{-1}), C-H stretching (3000 to 2800 cm^{-1}), O-H/C-H bending (1800 to 1500 cm^{-1}), C-O stretching (1239.2 cm^{-1}), V = O/W = O stretching (1100 to 950 cm^{-1}), and V-O/W-O stretching (700 to 400 cm^{-1}). We found that the FT-IR spectrum of W-VEG prepared at the 1:1 mixing ratio of EG to 1-dodecanol was distinctly different from those of other W-VEGs. When we observed the C-H stretching bands in the range of 3000 to 2800 cm^{-1}, the peak positions of W-VEGs prepared at 1:1 were around 2958.6, 2925.8, and 2853.5 cm^{-1} while those at 1:0, 1:0.5, and 1:2 appeared at around 2958.6, 2940.3, and 2879.5 cm^{-1}, as shown in Figure 3b. The IR bands that appeared in the range of 1800 to 1500 cm^{-1} are ascribed to the overlapping spectra of O-H bending (~1670–1620 cm^{-1}) and C-H bending in the EG units (~ 1598 cm^{-1}) [25–27]. In Figure 3c, a shoulder peak in the range of 1790 to 1700 cm^{-1} appeared for W-VEG at the 1:1 mixing ratio, while only a strong band centered at around 1638 cm^{-1} was shown for all the other W-VEGs at the 1:0, 1:0.5, and 1:2 ratios. In addition, a strong IR band characteristic for C-O stretching appeared at 1239.2 cm^{-1} and a shoulder appeared at around 1286 cm^{-1} in the FT-IR spectrum of W-VEG at the 1:1 ratio. In contrast, two independent peaks at 1253.6 and 1231.5 cm^{-1} appeared in the FT-IR spectra of W-VEGs at the 1:0, 1:0.5, and 1:2 ratios. All these variations in the FT-IR spectrum of W-VEG at the 1:1 ratio strongly suggest that the dodecyloxy moiety combined with $WOCl_4$ was incorporated into the W-VEG structure, thereby distinctly changing the peak positions of C-H stretching, O-H/C-H bending, and C-O stretching. One of the most plausible mechanisms to explain these results can be the reaction of NH_4VO_3 and EG with $WOCl_4$ combined with both EG and 1-dodecanol to form W-VEG.

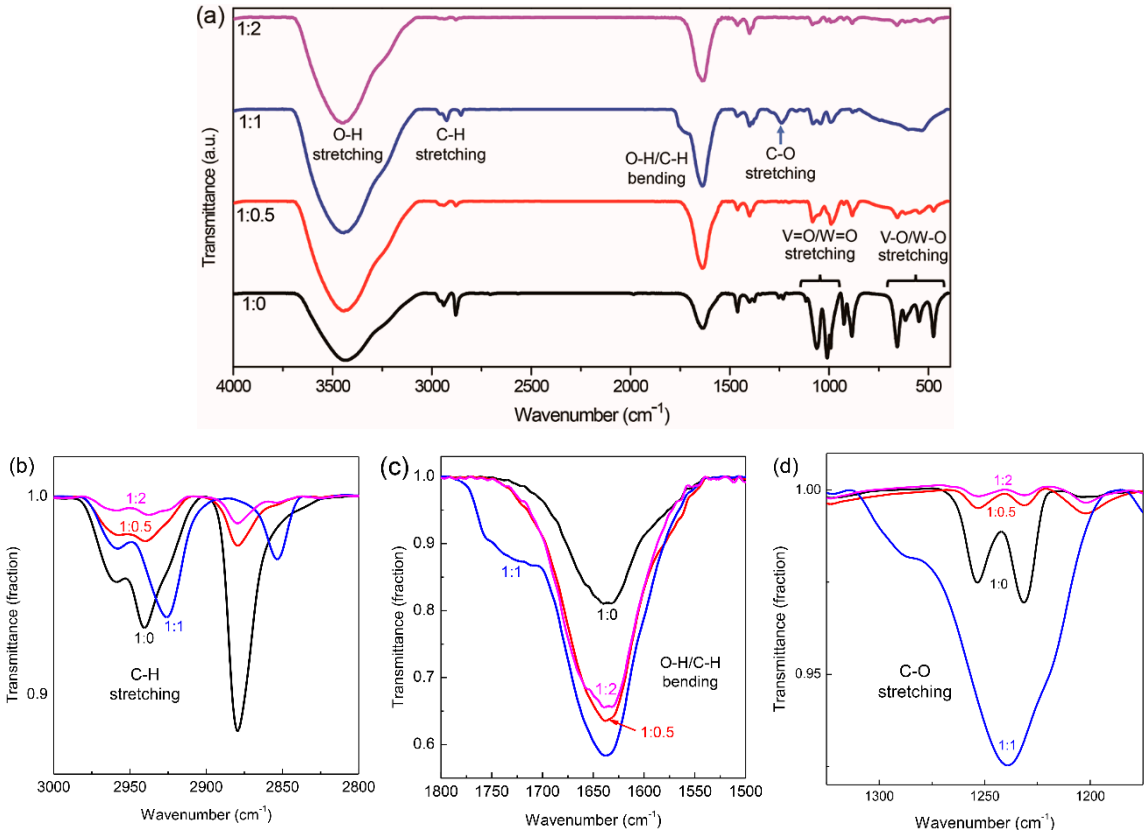

Figure 3. (**a**) FT-IR spectra of W-VEGs obtained with different mixing ratios of EG to 1-dodecanol at ratios of 1:0, 1:0.5, 1:1, and 1:2 at a fixed $WOCl_4$ concentration of 2.77 mol% relative to NH_4VO_3, and enlarged spectra of (**b**) C-H stretching, (**c**) O-H/C-H bending and (**d**) C-O stretching.

Then, we investigated the effects of the amount of tungsten precursor on the changes in the MIT temperature of W_xVO_2. We fixed the molar mixing ratio of EG to 1-dodecanol at 1:1 for further investigation. At the fixed conditions of NH_4VO_3, EG, and 1-dodecanol, the increasing concentrations of $WOCl_4$ were used for the synthesis of W_xVO_2. All XRD patterns of W_xVO_2 synthesized at 0, 2.77, 5.53, and 11.08 mol% of $WOCl_4$ to NH_4VO_3 in Figure 4a show that the VO_2 (M) phase (JCPDS No. 43-1051) was successfully synthesized, although there exists a portion of the V_6O_{13} phase with the addition of $WOCl_4$. With the further addition of $WOCl_4$ beyond 11.08 mol%, only V_6O_{13} was synthesized (data not shown), indicating the oxidation of VO_2 (M) due to the excessive addition of $WOCl_4$. The MIT temperatures decreased from 68.07, 61.23, and 56.95 down to 51.12 °C at $WOCl_4$ concentrations of 0, 2.77, 5.53, and 11.08 mol%, respectively, clearly showing the effects of tungsten doping (Figure 4b). This decrease in the MIT temperature is ascribed to the formation of the rutile phase VO_2 (R) with the W doping, as indicated in literature [28]. The enhancement of (110) peak at $2\theta = 26.8°$ is characteristic for the VO_2 (R) phase [28], and clearly shown in the XRD patterns of W_xVO_2, supporting this mechanism. It should also be noted that the full width at half maximum (FWHM) of the melting transitions in the DSC thermograms (Figure 4b) drastically increased with the addition of $WOCl_4$ from 3.9, 4.4, 6.2, to 11.4 °C. These results show that the crystallinity of W_xVO_2 was significantly decreased with increasing concentrations of $WOCl_4$. Furthermore, the intensity of the melting peak drastically decreased with the increasing W doping, indicating that the activation energy for the MIT was reduced. In the monoclinic VO_2 structure, V-V intervals are alternative (2.65 and 3.12 Å) while those in the rutile VO_2 above the MIT are symmetric (2.87 Å). When V atoms are partially substituted with W atoms, the V-V intervals are shrunk, decreasing the structural differences between the monoclinic and rutile structure, and thereby reducing the activation energy [29]. The amounts of tungsten doped to vanadium in W_xVO_2 (M) were 0.33, 0.97, and 2.07 mol%, as determined by ICP-AES

measurements (Table 1). These figures represent significantly decreased amounts in comparison to the tungsten precursor $WOCl_4$. Hereafter, the calcinated W_xVO_2 from W-VEGs prepared at $WOCl_4$ concentrations of 0, 2.77, 5.53, and 11.08 mol% are denoted by $W_{0.0033}VO_2$, $W_{0.0097}VO_2$, and $W_{0.0207}VO_2$, respectively. Our results showed that only 10~20% of tungsten added into the reaction mixtures was incorporated into the final W_xVO_2 compounds and indicate that a significant portion of $WOCl_4$ that reacted with EG and 1-dodecanol did not participate in the formation of W-VEGs. We presumed that many of the species shown in Scheme 2 might not be appropriate for the formation of W-VEGs.

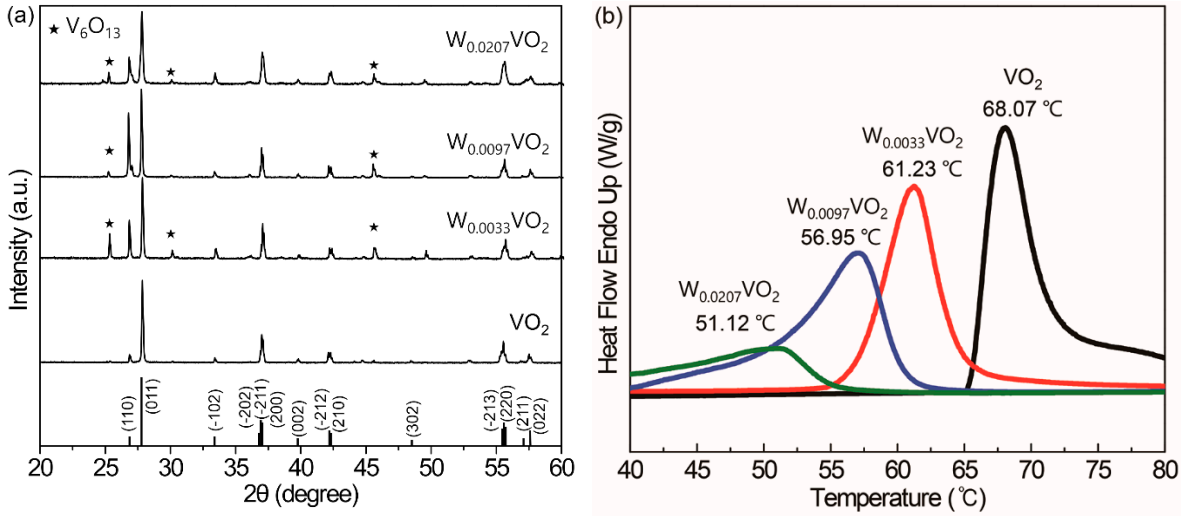

Figure 4. (**a**) XRD patterns and (**b**) DSC thermograms of tungsten-doped vanadium oxides obtained with different tungsten doping concentrations.

Table 1. Compositions of tungsten in the reaction mixture and calcined W_xVO_2 estimated by ACP-IES.

W in Reaction Mixtures (mol%)	W in W_xVO_2 (mol%)
2.77	0.33
5.53	0.97
11.08	2.07

To examine the origination of these broadening melting peaks resulting from an increase in the $WOCl_4$, we analyzed W-VEGs by measuring SEM images. Figure 5a shows that the VEG synthesized at the 1:1 mixing ratio of EG to 1-dodecanol without adding the $WOCl_4$. The VEG has a nanowire morphology with a square or rectangular cross section. The nanowire morphology with a high aspect ratio over 10 is clearly different from that of VEG with a nanorod or microrod morphology prepared without using 1-dodecanol, which can be observed in Figure 2a. These results demonstrate that 1-dodecanol acts as a capping agent to block a specific crystal plane, thereby enhancing one-dimensional growth when VEG is synthesized. With the addition of $WOCl_4$, the nanowire morphology disappears, presenting irregular crystal morphologies, as shown in Figure 5b–d. The crystal sizes of W-VEGs decreased from the micrometer-scale at 2.77 mol% to the nanometer-scale at 5.53 and 11.08 mol% of $WOCl_4$, as shown in Figure 5b–d, respectively. We ascribe this disappearance of the nanowire morphology and the decrease in the crystal sizes to the increasing portion of dodecyloxy moieties in W-VEGs. When the bulky alkyl side chains are incorporated into the crystal structure of W-VEGs, they might act as defects to the formation of the one-dimensional chain-like structures shown in Scheme 1 and the crystallization of the chains.

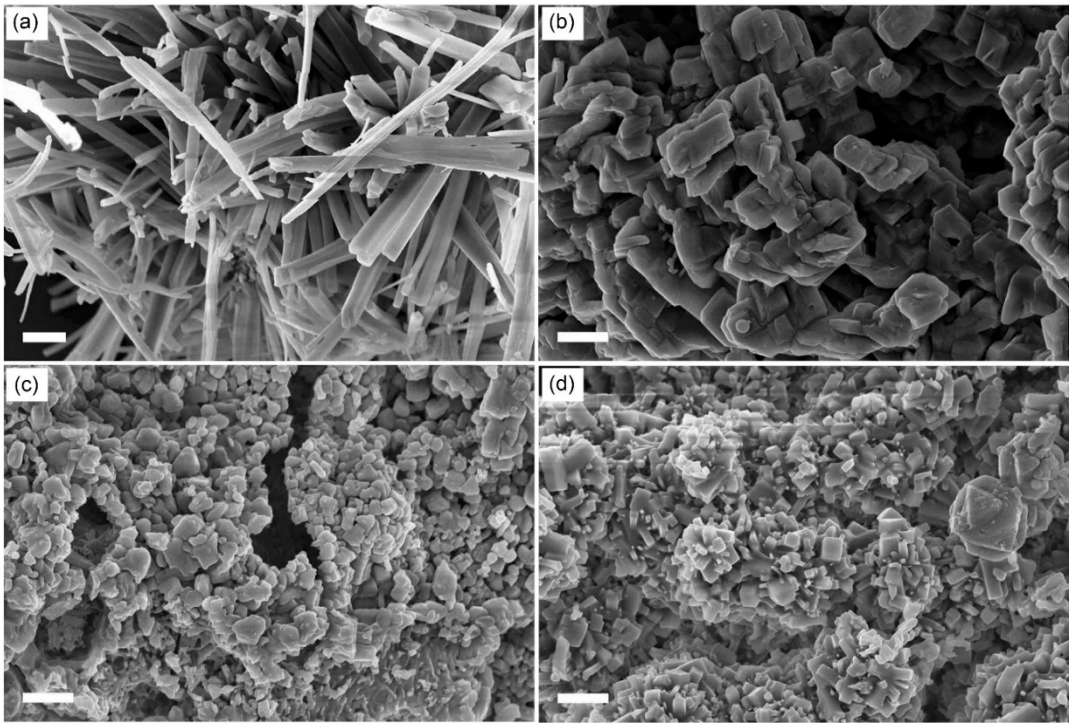

Figure 5. FE-SEM images of W-VEGs obtained with different $WOCl_4$ concentrations at (**a**) 0, (**b**) 2.77, (**c**) 5.53, and (**d**) 11.08 mol% relative to NH_4VO_3 at the fixed ratio of EG to 1-dodecanl at 1:1. (scale bar = 1 μm).

W_xVO_2 compounds prepared via our modified polyol method utilizing 1-dodecanol present distinct thermochromic properties. We measured the transmittance spectra of the VO_2 and $W_{0.0207}VO_2$ crystals dispersed in ethanol at 20 and 70 °C as two representatives. When the UV-Vis-NIR curves of 20 and 70°C were compared, there were no significant changes in the range of visible light shorter than 780 nm. However, in the NIR region, we observed that the transmittances of ethanol dispersions of VO_2 and $W_{0.0207}VO_2$ at 70 °C were significantly decreased from those at 20 °C. The solar modulation T_{sol} at each temperature was calculated by Equation (1), where $\varphi(\lambda)$ and $Tr(\lambda)$ are the solar irradiation spectrum for an air mass of 1.5 (corresponding to the sun standing 37° above the horizontal) [30] and transmittance at specific wavelengths λ, respectively, and ΔT_{sol} was estimated by Equation (2) [9]. The luminous transmittance was also calculated by Equation (3) where $\varphi_{lum}(\lambda)$ is the spectral sensitivity of the light-adapted eye [18]. The estimated ΔT_{sol} of VO_2 without tungsten doping was 2.5% and that of $W_{0.0207}VO_2$ was 21.8%. The usefulness of our modified polyol method utilizing $WOCl_4$ and 1-dodecanol to prepare tungsten-doped VO_2 is evidenced by the significantly enhanced solar modulation of the ethanol dispersion of $W_{0.0207}VO_2$ with the manifestation of the tungsten doping. The luminous transmittance of $W_{0.0207}VO_2$ at 20 °C estimated by Equation (3) was 66.8% while that of VO_2 was 78.2%. This decrease in the luminous transmittance with the tungsten doping can be ascribed to serious light scattering of $W_{0.0207}VO_2$ in comparison to VO_2. Sizes of VO_2 and $W_{0.0207}VO_2$ nanoparticles estimated by analyzing their SEM images shown in Figure 6c,d are 156 ± 81 and 287 ± 84 nm, respectively. These results indicate that the $W_{0.0207}VO_2$ nanoparticles with bigger sizes than the VO_2 nanoparticles significantly scatter light, resulting in the decrease in transmittance. It should be noted that the average crystallite sizes of VO_2 and V_6O_{13} estimated by using XRD patterns in Figure 4a and the Scherrer equation [31] are 63.8 and 36.2 nm, respectively. The bigger size of the $W_{0.0207}VO_2$ nanoparticles than their crystallite sizes indicate that the nanoparticles have polycrystalline textures. On the other hand, the thermochromic properties gained in our study are compared with those of W_xVO_2 with the MIT temperature (T_c) in a range of 40–45 °C in Table 2. The T_{lum} at 20 °C and ΔT_{sol} of $W_{0.0207}VO_2$ in this study are higher than those of reported materials except the T_{lum} at 20 °C of the W-doped

VO_2/polyvinylpyrrolidone coating as presented in the Table 2 [32–35]. This comparison suggests that W_xVO_2 materials in our study have a great potential for thermochromic applications.

$$T_{sol} = \frac{\int \varphi(\lambda) \cdot Tr(\lambda) \cdot d\lambda}{\int \varphi(\lambda) \cdot d\lambda} \quad (1)$$

$$\Delta T_{sol} = T_{sol}(20\,^{\circ}\mathrm{C}) - T_{sol}(70\,^{\circ}\mathrm{C}) \quad (2)$$

$$T_{lum} = \frac{\int \varphi_{lum}(\lambda) \cdot Tr(\lambda) \cdot d\lambda}{\int \varphi_{lum}(\lambda) \cdot d\lambda} \quad (3)$$

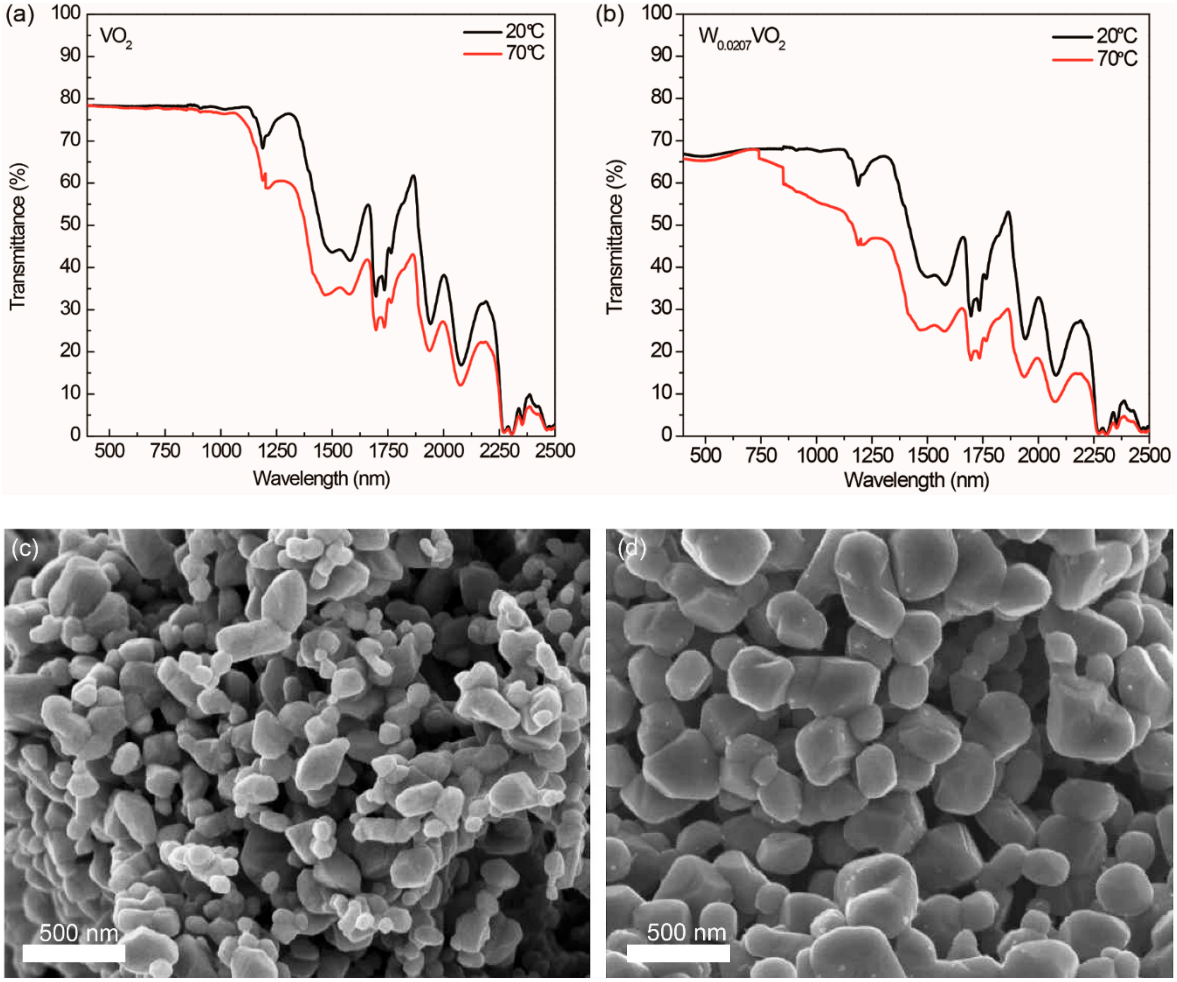

Figure 6. Transmittance spectra of ethanol dispersions of (**a**) VO_2 and (**b**) $W_{0.0207}VO_2$, and SEM images of (**c**) VO_2 and (**d**) $W_{0.0207}VO_2$ nanoparticles.

Table 2. A summary of thermochromic properties of tungsten-doped VO_2.

Samples	W in W_xVO_2 (%)	T_c (°C)	T_{lum} at 20 °C (%)	ΔT_{sol} (%)	Ref.
Mesoporous film	0.4	43.0	61.6	11.4	[31]
Coating with PVP	3	44.4	68.3	20.4	[32]
Core@SiO_2 shell	2	43.0	39.1	12.9	[33]
NP Film	0.7	42.7	63.4	11.7	[34]
Dispersion	2.07	51.1	66.8	21.8	This study

4. Conclusions

In this study, we carried out the synthesis of tungsten-doped VO_2 via a polyol method based on ammonium metavanadate and EG by utilizing $WOCl_4$ and 1-dodecanol as the tungsten source and capping agent, respectively. By conducting extensive characterizations using XRD, DSC, SEM, FT-IR, UV-Vis-NIR spectroscopy, and ICP-AES analysis, it was suggested that $WOCl_4$ coupled with both EG and 1-dodecanol at an optimal ratio was responsible for the successful incorporation of tungsten into W-VEG in the creation of the calcinated compound, W_xVO_2. Other popular tungsten sources such as WCl_6 and Na_2WO_4 were not effective for the tungsten doping in the polyol process, which indicates the usefulness of our modified polyol method that utilizes 1-dodecanol and $WOCl_4$. However, it should be noted that the incorporation of bulky dodecyl chains into W-VEG seems to result in an increased FWHM value for the melting transition and that the current MIT temperature of W_xVO_2 at around 51 °C should be further decreased to near room temperature for practical thermochromic applications. In addition, the decrease in the luminous transmittance with the tungsten doping should be improved. These issues suggest that further investigations should be undertaken to find alcohol capping agents less bulky than 1-dodecanol and processes to avoid aggregations.

Author Contributions: Conceptualization, Y.L. and J.P.; Y.L.; investigation, Y.L., S.W.J. and S.H.P.; writing—original draft preparation, Y.L.; writing—review and editing, J.W.Y. and J.P.; visualization, S.W.J.; supervision, J.P.; project administration, Y.L. and S.H.P.; funding acquisition, J.W.Y. and J.P. All authors have read and agreed to the published version of the manuscript.

Funding: This research was supported by the Chung-Ang University Graduate Research Scholarship in 2018 and the Korea Institute of Energy Technology Evaluation and Planning, funded by the Ministry of Trade, Industry and Energy (Grant No. 20182020109500), Korea.

Acknowledgments: The authors thank the Korea Basic Science Institute (KBSI) for the FT-IR and ICP-AES measurements.

Conflicts of Interest: The authors declare no conflict of interest.

References

1. Gao, Y.; Luo, H.; Zhang, Z.; Kang, L.; Chen, Z.; Du, J.; Kanehira, M.; Cao, C. Nanoceramic VO_2 thermochromic smart glass: A review on progress in solution processing. *Nano Energy* **2012**, *1*, 221–246. [CrossRef]
2. Qazilbash, M.M.; Brehm, M.; Chae, B.G.; Ho, P.C.; Andreev, G.O.; Kim, B.J.; Yun, S.J.; Balatsky, A.V.; Maple, M.B.; Keilmann, F.; et al. Mott transition in VO_2 revealed by infrared spectroscopy and nano-Imaging. *Science* **2007**, *318*, 1750–1753. [CrossRef]
3. Morin, F.J. Oxides which show a metal-to-insulator transition at the Neel temperature. *Phys. Rev. Lett.* **1959**, *3*, 34. [CrossRef]
4. Vostakola, M.F.; Yekta, B.E.; Mirkazemi, S.M. The Effects of vanadium pentoxide to oxalic acid ratio and different atmospheres on the formation of VO_2 aanopowders synthesized via sol–gel method. *J. Electron. Mater.* **2017**, *46*, 6689–6697. [CrossRef]
5. Ji, C.; Wu, Z.; Wu, X.; Feng, H.; Wang, J.; Huang, Z.; Zhou, H.; Yao, W.; Gou, J.; Jiang, Y. Optimization of metal-to-insulator phase transition properties in polycrystalline VO_2 films for terahertz modulation applications by doping. *J. Mater. Chem. C* **2018**, *6*, 1722–1730. [CrossRef]
6. Li, M.; Magdassi, S.; Gao, Y.; Long, Y. Hydrothermal synthesis of VO_2 polymorphs: Advantages, challenges and prospects for the application of energy efficient smart windows. *Small* **2017**, *13*, 1701147. [CrossRef]
7. Peng, Z.; Jiang, W.; Liu, H. Synthesis and electrical properties of tungsten-doped vanadium dioxide nanopowders by thermolysis. *J. Phys. Chem. C.* **2007**, *111*, 1119–1122. [CrossRef]
8. Chang, T.-C.; Cao, X.; Bao, S.-H.; Ji, S.-D.; Luo, H.-J.; Jin, P. Review on thermochromic vanadium dioxide based smart coatings: From lab to commercial application. *Adv. Manuf.* **2018**, *6*, 1–19. [CrossRef]
9. Choi, Y.; Sim, D.M.; Hur, Y.H.; Han, H.J.; Jung, Y.S. Synthesis of colloidal VO_2 nanoparticles for thermochromic applications. *Sol. Energ. Mater. Sol. C* **2018**, *176*, 266–272. [CrossRef]
10. Li, G.; Chao, K.; Peng, H.; Chen, K.; Zhang, Z. Low-valent vanadium oxide nanostructures with controlled crystal structures and morphologies. *Inorg. Chem.* **2007**, *46*, 5787–5790. [CrossRef]

11. Binions, R.; Hyett, G.; Piccirillo, C.; Parkin, I.P. Doped and un-doped vanadium dioxide thin films prepared by atmospheric pressure chemical vapour deposition from vanadyl acetylacetonate and tungsten hexachloride: The effects of thickness and crystallographic orientation on thermochromic properties. *J. Mater. Chem.* **2007**, *17*, 4652–4660. [CrossRef]
12. Batista, C.; Ribeiro, R.; Carneiro, J.; Teixeira, V. DC sputtered W-doped VO_2 thermochromic thin films for smart windows with active solar control. *J. Nanosci. Nanotechnol.* **2009**, *9*, 4220–4226. [CrossRef]
13. Jin, P.; Tazawa, M.; Ikeyama, M.; Tanemura, S.; Macak, K.; Wang, X.; Olafsson, S.; Helmersson, U. Growth and characterization of epitaxial films of tungsten-doped vanadium oxides on sapphire (110) by reactive magnetron sputtering. *J. Vac. Sci. Technol.* **1999**, *17*, 1817–1821. [CrossRef]
14. Mabakachaba, B.; Madiba, I.; Kennedy, J.; Kaviyarasu, K.; Ngoupe, P.; Khanyile, B.; Van Rensburg, J.; Ezema, F.; Arendse, C.; Maaza, M. Structural and electrical properties of Mg-doped vanadium dioxide thin films via room-temperature ion implantation. *Surf. Interfaces* **2020**, *20*, 100590. [CrossRef]
15. Zou, J.; Peng, Y.; Lin, H. A low-temperature synthesis of monoclinic VO_2 in an atmosphere of air. *J. Mater. Chem. A* **2013**, *1*, 4250–4254. [CrossRef]
16. Kim, H.J.; Roh, D.K.; Jung, H.S.; Kim, D.-S. Size and shape control of monoclinic vanadium dioxide thermochromic particles for smart window applications. *Ceram. Int.* **2019**, *45*, 4123–4127. [CrossRef]
17. Feldmann, C. Polyol-mediated synthesis of nanoscale functional materials. *Adv. Funct. Mater* **2003**, *13*, 101–107. [CrossRef]
18. Zhang, H.; Xiao, X.; Lu, X.; Chai, G.; Sun, Y.; Zhan, Y.; Xu, G. A cost-effective method to fabricate VO_2 (M) nanoparticles and films with excellent thermochromic properties. *J. Alloys Compd.* **2015**, *636*, 106–112. [CrossRef]
19. Weeks, C.; Song, Y.; Suzuki, M.; Chernova, N.A.; Zavalij, P.Y.; Whittingham, M.S. The one dimensional chain structures of vanadyl glycolate and vanadyl acetate. *J. Mater. Chem.* **2003**, *13*, 1420–1423. [CrossRef]
20. Yao, M.-M.; Jiang, C.-H.; Yao, J.-S.; Wang, K.-H.; Chen, C.; Yin, Y.-C.; Zhu, B.-S.; Chen, T.; Yao, H.-B. General Synthesis of Lead-Free Metal Halide Perovskite Colloidal Nanocrystals in 1-Dodecanol. *Inorg. Chem.* **2019**, *58*, 11807–11818. [CrossRef]
21. Jo, C.W.; Kim, H.J.; Yoo, J.W. Thermochromic Properties of W-Mo Co-Doped VO_2 (M) Nanoparticles According to Reaction Parameters. *J. Nanosci. Nanotechnol.* **2017**, *17*, 2923–2928. [CrossRef]
22. Zhang, Y.; Huang, C.; Meng, C. Controlled synthesis of V_6O_{13} nanobelts by a facile one-pot hydrothermal process and their effect on thermal decomposition of ammonium perchlorate. *Mater. Express* **2015**, *5*, 105–112. [CrossRef]
23. Guan, S.; Rougier, A.; Viraphong, O.; Denux, D.; Penin, N.; Gaudon, M. Two-step synthesis of VO_2 (M) with tuned crystallinity. *Inorg. Chem.* **2018**, *57*, 8857–8865. [CrossRef]
24. Li, Q.; Zhu, Y.; Yu, Y.; Qian, Y. Synthesis and Transformation of Vanadyl Ethylene Glycolate, and Their Applications in a Lithium-Ion Battery. *Int. J. Electrochem. Sci.* **2012**, *7*, 5557–5564.
25. Ai, L.; Wang, Z.; He, F.; Wu, Q. Synthesis and conductive performance of polyoxometalate acid salt gel electrolytes. *RSC Adv.* **2018**, *8*, 34116–34120. [CrossRef]
26. Ragupathy, P.; Shivakumara, S.; Vasan, H.; Munichandraiah, N. Preparation of nanostrip V_2O_5 by the polyol method and its electrochemical characterization as cathode material for rechargeable lithium batteries. *J. Phys. Chem. C* **2008**, *112*, 16700–16707. [CrossRef]
27. Partheeban, T.; Sasidharan, M. Template-free synthesis of LiV_3O_8 hollow microspheres as positive electrode for Li-ion batteries. *J. Mater. Sci.* **2020**, *55*, 2155–2165. [CrossRef]
28. Liang, S.; Shi, Q.; Zhu, H.; Peng, B.; Huang, W. One-step hydrothermal synthesis of W-doped VO_2 (M) nanorods with a tunable phase-transition temperature for infrared smart windows. *ACS Omega* **2016**, *1*, 1139–1148. [CrossRef]
29. Li, D.; Li, M.; Pan, J.; Luo, Y.; Wu, H.; Zhang, Y.; Li, G. Hydrothermal Synthesis of Mo-Doped VO_2/TiO_2 Composite Nano crystals with Enhanced Thermochromic Performance. *ACS Appl. Mater. Interfaces* **2014**, *6*, 6555–6561. [CrossRef]
30. American Society for Testing and Materials. *ASTM G173-03 Standard Tables of Reference Solar Spectral Irradiances: Direct Normal and Hemispherical on a 37° Tilted Surface*; American Society for Testing and Materials: Philadelphia, PA, USA, 2020.
31. Nath, D.; Singh, F.; Das, R. X-ray diffraction analysis by Williamson-Hall, Halder-Wagner and size-strain plot methods of CdSe nanoparticles—A comparative study. *Mater. Chem. Phys.* **2020**, *239*, 122021. [CrossRef]

32. Li, B.; Tian, S.Q.; Tao, H.Z.; Zhao, X.J. Tungsten doped M-phase VO_2 mesoporous nanocrystals with enhanced comprehensive thermochromic properties for smart windows. *Ceram. Int.* **2019**, *45*, 4342–4350. [CrossRef]
33. Zomaya, D.; Xu, W.Z.; Grohe, B.; Mittler, S.; Charpentier, P.A. W-doped VO_2/PVP coatings with enhanced thermochromic performance. *Sol. Energy Mater. Sol. Cells* **2019**, *200*, 109900. [CrossRef]
34. Chen, R.; Miao, L.; Cheng, H.L.; Nishibori, E.; Liu, C.Y.; Asaka, T.; Iwamoto, Y.; Takata, M.; Tanemura, S. One-step hydrothermal synthesis of $V_{1-x}W_xO_2$ (M/R) nanorods with superior doping efficiency and thermochromic properties. *J. Mater. Chem. A* **2015**, *3*, 3726–3738. [CrossRef]
35. Zhang, L.; Xia, F.; Yao, J.; Zhu, T.; Xia, H.; Yang, G.; Liu, B.; Gao, L. Facile synthesis, formation mechansm and thermochromic properties of W-doped VO_2(M) nanoparticles for smart window applications. *J. Mater. Chem. C* **2020**, *8*, 13396. [CrossRef]